PROCEEDINGS, 48th Workshop on Geothermal Reservoir Engineering
Stanford University, Stanford, California, February 6-8, 2023
SGP-TR-224

Effect of thermal and mechanical processes on hydraulic transmissivity evolution

Tamara Jeppson, David Lockner, Joshua Taron, Diane Moore, Brian Kilgore, Nicholas Beeler, and Stephen Hickman

U.S. Geological Survey, Earthquake Science Center, 345 Middlefield Rd. MS977, Menlo Park, CA 94025

tjeppson@usgs.gov

Keywords: Fluid-rock interactions, shear fractures, sealing, hydraulic transmissivity

ABSTRACT

Fracture healing is a critical component of enhanced geothermal systems, the earthquake cycle, and induced seismicity. Accordingly, there is significant interest in understanding the process of healing and its effects on fluid transport. The creation, reactivation, and sustainability of fracture networks depend on complex coupling among thermal, hydraulic, mechanical, and chemical processes. We performed laboratory slide-hold-slide experiments, at temperatures from 22 to 200 ˚C, to examine effects of fracture reactivation and quasi-static loading on the evolution of fluid transport properties of simulated fractures in Westerly granite. At all temperatures, the in-plane hydraulic transmissivity consistently decays during hold periods resulting in an overall reduction in transmissivity. During the first 3 to 15 hours of an experiment, transmissivity decreases rapidly due to the generation of wear products, development of a sliding surface, and compaction of the resulting gouge. Once the sliding surface has developed, the long-term transmissivity decay rate at 22 and 100 ˚C is significantly lower than the transmissivity decay rate during the initial 3 to 7 hours of the experiment. However, at 200 °C, the decay of hydraulic transmissivity remains high throughout the experiment. The long-term decay of hydraulic transmissivity can be fitted with a power law model with more rapid reduction of hydraulic transmissivity at higher temperature. Periods of sliding on the fracture surface result in transient increases in the transmissivity, due to shear dilation, as is expected for Coulomb materials. These transients are superimposed on the long-term decay. When sliding ceases and a new hold period commences, there is a rapid reduction in transmissivity and return to the long-term rate of transmissivity decay. The rate of decay of the transmissivity transients is inversely proportional to temperature, in contrast to the long-term decay and the expected behavior for processes like subcritical crack growth and indentation creep. The higher decay rates that are observed during the initial 3 to 15 hours of the tests and following sliding, are associated with times that the porosity of the gouge is expected to be high. The difference in decay rates suggests that when the gouge is driven far from equilibrium by active shearing, densification may be dominated by a different mechanism from long-term compaction.

1. INTRODUCTION

The presence of large-scale fracture networks in the upper crust is critical to the success of enhanced geothermal system (EGS) reservoirs. Whether naturally occurring or created, fracture systems gradually seal over time leading to reduced fluid flow (Kitagawa et al., 2002; Manga et al., 2012; Xue et al., 2013), affecting the productivity and longevity of geothermal reservoirs. Fluid flow can be enhanced by reactivation of faults within a reservoir (*e.g.,* Hickman et al., 1998; Chabora et al., 2012; Plummer et al., 2016), but while shear stimulation methods are generally effective at increasing fluid flow in EGS, the magnitude of the enhancement and its persistence over time, especially at elevated temperatures and in the presence of chemical disequilibrium, are poorly understood.

The evolution of the fluid transport properties of fractures has been examined in laboratory experiments. Many of these studies focus on how the fluid transport properties evolve in static fractures at different temperatures (25 to 500 ˚C), quantifying the rates of permeability decay over time (Moore et al., 1994; Morrow et al., 2001; Polak et al; 2003; Farough et al., 2016). These studies indicate that permeability reduction at elevated temperature is primarily the result of solution-transfer processes, with rock dissolution at asperities reducing the fracture aperture and secondary mineral precipitation filling pores. Other studies have examined the effect of shearing on the evolution of fluid transport properties for bare-surface (Zhang and Tullis, 1998; Fang et al., 2017; Im et al., 2018, 2019; Acosta et al., 2022) and gouge-filled (Olsen et al., 1998; Zhang and Tullis, 1998; Zhang et al., 1999; Crawford et al, 2008; Faulkner et al., 2018) fractures. Some of these studies examined how permeability evolves with continuous shear displacement at room temperature, showing that there is an initial drastic reduction in permeability with the onset of shearing due to grain crushing (Zhang and Tullis, 1998). With continued shearing the permeability continues to decrease due to a combination of grain crushing and shear localization but the rate of permeability reduction slows (Zhang and Tullis, 1998). Other experiments at room temperature examined the evolution of fluid transport in fractures during cyclic periods of shearing and quasi-static holds. These studies found that permeability decays continuously during hold periods due to compaction, but when shear deformation resumes permeability often increased due to shear dilation. The magnitude of permeability gain increases with duration of the preceding hold period (Im et al., 2019).

Relatively little work has sought to examine the interplay between fluid transport properties and mechanical shearing at elevated temperatures where complex interactions among mechanical, hydraulic, chemical, and thermal processes will affect how fracture properties evolve. Tenthorey et al. (2003) acquired periodic permeability measurements in fractured sample of Fontainebleau sandstone during an experiment at 927 ˚C. Permeability decreases continuously with time during a 12 hour hold but no measurements were acquired while the fracture was being sheared. Olsen et al. (1998) continuously recorded permeability in a gouge composed of a mixture of quartz and labradorite at temperatures of 25 to 250 ˚C during both periods of shearing and holding. They observed little to no change in permeability at temperatures < 100 ˚C but saw a clear decrease in permeability at temperatures ≥ 200 ˚C. Slight increases in permeability

accompanied shearing but the amount of increase was independent of the duration of the preceding hold period, in contrast to tests at room temperature.

Understanding the evolution of fluid transport properties in shear fractures at elevated temperatures, representative of enhanced geothermal systems (EGS) is required to create the most efficient and sustainable EGS reservoirs and model their performance over time. To this end, we present the results of experiments examining the combined effect of temperature and shear deformation on the evolution of hydraulic transmissivity in simulated, initially bare-surface, fractures in Westerly granite at hydrothermal conditions.

2. METHODS

Along-fault flow-through experiments were conducted using 25.4 mm diameter cylindrical samples of Westerly granite (~ 61 mm long) cut at a 30˚ angle relative to the sample axis. The cut surfaces were ground flat and roughened with #240 grit sandpaper to attain similar starting surfaces with an RMS roughness of ~ 4 μm. Offset boreholes (2.38 mm-diameter) drilled into each sample half provide fluid access to the simulated fracture surface.

Experiments were performed in the conventional triaxial configuration used in frictional shearing experiments (Figure 1). The triaxial apparatus is internally heated and uses argon gas as the confining medium. Samples were jacketed against the confining medium using lead tubes with a 1.0 mm wall thickness. A constant confining pressure of 30 MPa was applied, and an external load cell was used to measure the axial load with a precision of 0.1 MPa. In all tests, the sample and pore pressure system were evacuated before application of confining pressure. Deionized water was then introduced, and pore pressure was generally fixed at 11 MPa at the inlet at the top of the sample and at 9 MPa at the outlet on the bottom. However, in some experiments, especially early in the tests, the permeability was too high for the pore pressure pump to produce this gradient resulting in a lower pore pressure differential. In high-temperature experiments, a resistance heater was placed around the sample assembly inside the pressure vessel. Calibration tests define the temperature profile produced by the heater and alumina spacers are sized so that the middle of the rock sample was positioned at the peak temperature. The temperature at either end of the sawcut was 2.3 % lower than the temperature at the middle. The temperature was raised over a period of 40 to 60 minutes and was monitored by a thermocouple inserted through the borehole to the top of the granite sample. During the experiment the temperature was typically maintained to within ± 0.5 ˚C with occasional fluctuations up to ± 2 ˚C. The piston was advanced at a rate of 1 μm/s for 0.9 mm of axial displacement then the rate was decreased to 0.1 μm/s for an additional 0.1 mm of displacement, corresponding to ~ 0.97 mm of shear displacement on the sawcut surface. During this initial sliding interval, a thin layer of ultrafine gouge develops (*e.g.,* Lockner et al., 2017). The piston position was then fixed for a predetermined interval of time before sliding resumed at a rate of 0.1 μm/s for 0.25 mm of axial displacement. This sequence of slide and hold periods continued in a similar manner, with holds, ranging in duration from 100 to 500,000 s (~ 5.8 days) and occurring after every 0.25 mm of axial displacement. A greased Teflon shim, placed between the sample assembly and the piston, accommodates the lateral slip of the lower half of the sample.

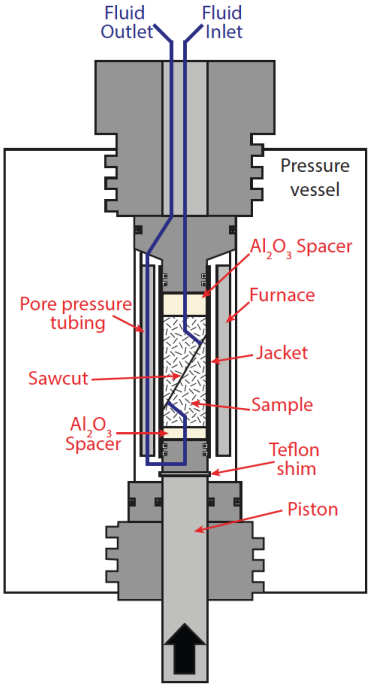

Figure 1. Schematic of the triaxial apparatus and sample geometry used in this study. Figure not to scale. Black arrow indicates the loading direction.

The change in fluid volume in the pore pressure pumps was recorded continuously and used to determine the average flow rate over 15-minute intervals. Because this flow rate was based on the volume of water at room temperature, it is adjusted for flow through the heated sample by

$$Q_T = Q_{22^\circ}\left({}^{V_T}/_{V_{22^\circ}}\right) \quad (1)$$

Where Q is the volumetric flow rate and V is the specific volume of water with the subscript denoting the temperature in degrees Celsius (Morrow et al., 2001). The lower limit for flow-rate measurements in the system is $1x10^{-8}$ ml/s.

For a fracture-dominated system, the measured flow rate is affected by the fracture aperture which we do not measure directly. For this reason, we define hydraulic transmissivity (κ) of the fracture, which we define as the product of permeability (k) and fracture aperture (a) with units of m^3. This definition of hydraulic transmissivity is commonly used in laboratory studies (e.g., Zimmerman and Bodvarsson, 1996), but is different than the definition of hydraulic transmissivity used in groundwater hydrology which is defined as the product of hydraulic conductivity and aperture with units of m^2/s (Hantush, 1964). Calculating the hydraulic transmissivity of the fracture is complicated by the elliptical geometry of the sawcut surface and the use of boreholes as fluid entry and exit points. Thus, we scribed grooves in the fracture surface (as described below) to facilitate plane-parallel flow and used a rectangular approximation, where a constant fracture width with parallel flow is assumed and hydraulic transmissivity ($\kappa_\parallel$) is estimated based on Darcy's law (e.g., Zimmerman and Bodvarsson, 1996):

$$\kappa_\parallel = {}^{v_f Q_T L}/_{w\Delta P} \quad (2)$$

where v_f is the dynamic viscosity of water at the experiment temperature (0.135 cP at 200 ˚C), L is the distance between the boreholes, which decreases with increasing shear displacement, ΔP is the pore pressure differential across the boreholes, and w is the width of the fracture. In our experiments a groove was scribed onto each sawcut surface, intersecting the boreholes perpendicular to the long axis of the sample. The groove length is used for w. In our initial experiments, the groove length was only 6-7 mm long but in E35 this length was increased to 16 mm. As the flow paths in the elliptical fracture are not truly parallel, even with the inscribed grooves, this approach overestimates the true hydraulic transmissivity (κ_{true}). We have run some preliminary finite-difference simulations using the actual sample geometry which indicate that true transmissivity is $\kappa_{true} \cong \kappa_\parallel/3$. In E35, the longer groove promotes flow paths that are closer to parallel, in which case $\kappa_{true} \cong \kappa_\parallel/1.5$. In the following analysis, we used these relations to estimate the true hydraulic transmissivity. However, since we are primarily interested in loss rate of transmissivity, which only depends on relative changes in κ, sample geometry should not have a significant impact on our analysis.

3. RESULTS

Figure 2 shows the evolution of hydraulic transmissivity during five experiments at three different temperatures (22, 100, and 200 ˚C) that lasted up to 16 days (Jeppson et al., 2023). In experiments E20 and E35 an initial hydraulic transmissivity for the unheated and unsheared fracture was measured and found to be $3x10^{-16}$ and $8x10^{-18}$ m^3, respectively. After 30 minutes at temperature and ~ 0.97 mm of shear displacement, the hydraulic transmissivity had dropped to $1x10^{-19}$ and $2x10^{-19}$ m^3, respectively. Hydraulic transmissivity decreases rapidly at all temperatures through the initial sequence of slides and holds. However, after 3 hours at 22 ˚C and 7 hours at 100 ˚C (corresponding to 1.7 and 2.1 mm of shear displacement) the rate of hydraulic transmissivity decrease slows. Subsequently, hydraulic transmissivity decreases at a slower and relatively uniform rate, interrupted only by transient increases in transmissivity that accompany shear. When the hydraulic transmissivity data are plotted on a log-log scale (Figure 2b) the transition in rate of reduction is clear. However, at 200 ˚C both the initial (< 15 hours, corresponding to 2.4 mm of shear displacement) and longer-term decay follow approximately the same trend (Figure 2b). The long-term rate of hydraulic transmissivity decrease can be quantified by a power-law equation of the form:

$$\kappa = At^{-R} \quad (3)$$

where A is a constant, t is time, and the exponent, R, is the power law rate used to quantify the transmissivity loss rate. The long-term loss rate is positively correlated with temperature, with an average R-value of 0.15, 0.24, and 0.63 at 22, 100, and 200 ˚C, respectively. At 22 and 100 ˚C there is about an order of magnitude reduction in the heated transmissivity over the course of the experiments; but, at 200 ˚C the final transmissivity is roughly two orders of magnitude below the initial heated value.

Superimposed on the long-term decay curve are transient increases in hydraulic transmissivity associated with sliding periods that occurred during the experiments. The increased transmissivity is followed by rapid decay and eventual return to the background long-term decay curve. During the first 3 to 7 hours (10,800 and 25,200 s) of the experiments clear increases in hydraulic transmissivity associated with sliding are not observed. Subtracting the long-term decay curve from the hydraulic transmissivity data highlights the transient behavior (Figure 3a). The decay of these residuals appears to be best described by an exponential decay model of the form:

$$\kappa_R = Ce^{-R_e t} \quad (4)$$

where κ_R is the residual of hydraulic transmissivity after removal of the long-term decay curve, C is a constant, and R_e is the exponential decay rate. In contrast to the long-term decay rates (Figure 2), the rate at which the transients decay exhibits a negative correlation with temperature (Figure 3b).

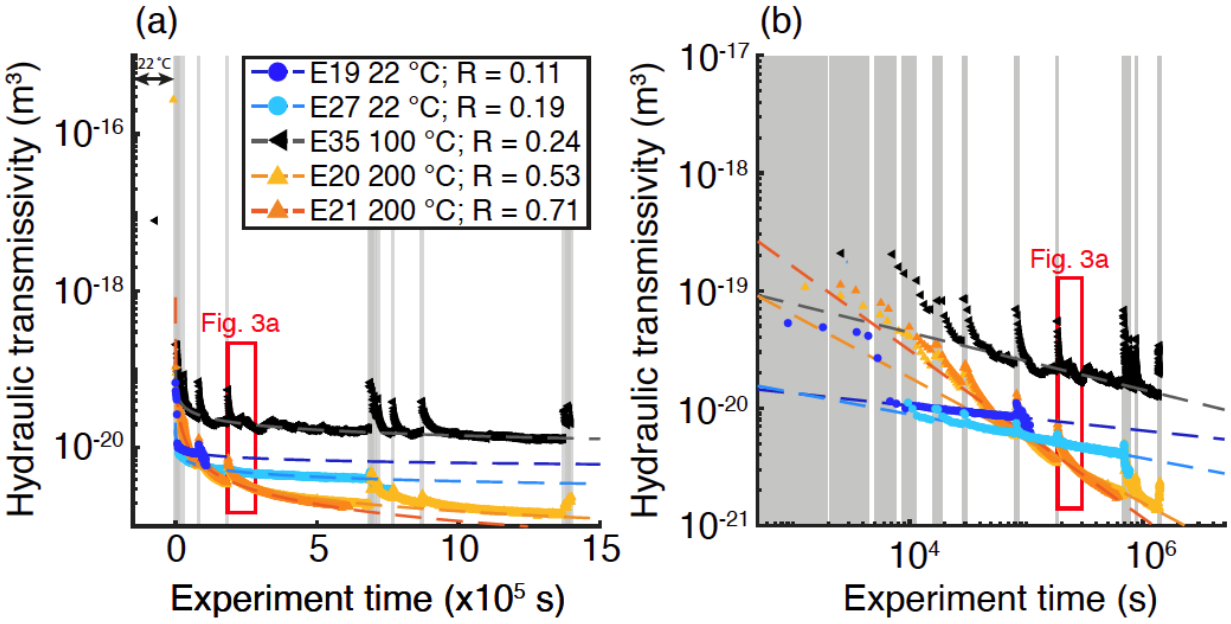

Figure 2. Evolution of hydraulic transmissivity with time, shown on a (a) log-linear and (b) log-log scale. Zero time marks the start of axial displacement. Flow-through experiments were conducted at 22 ˚C (blue circles), 100 ˚C (black triangles), and 200 ˚C (orange triangles). The long-term rate of transmissivity reduction is quantified by fitting a power law model (Eqn. 3, dashed lines). Vertical gray bars indicate sliding periods that commonly produce increases in transmissivity. Red box shows the time interval of the data shown in Figure 3a. Experiment E19 followed a different sequence of slides and holds than the other experiments shown but is included here to show the initial rapid decrease in hydraulic transmissivity.

We quantify the recovery (γ) of hydraulic transmissivity associated with the sliding periods as:

$$\gamma = \frac{\kappa_{slide}}{\kappa_{hold}} \tag{5}$$

where κ_{slide} is the maximum transmissivity during the sliding period and κ_{hold} is the transmissivity at the end of the preceding hold. This definition yields γ=1 when there is no change is transmissivity. The amount of recovery that occurs generally increases with duration of the previous hold period (Figure 4) and is similar at all temperatures for hold durations of less than $1\text{x}10^4$ s. For longer holds, recovery is greater at 100 ˚C than at 22 ˚C. The magnitude of recovery at 200 ˚C is split, with data acquired during the initial 52 hours ($\log(t)$ = 5.3; color scale in figure 4a) of both 200 ˚C experiments following the 100 ˚C trend and those from more than 52 hours (E20 only) following the 22 ˚C trend.

3.1 Microstructures

The sawcut surfaces of an experiment conducted at 200 ˚C were characterized using a scanning electron microscope (SEM). This sample had been removed from the triaxial vessel after 0.97 mm of slip followed by a $1.43\text{x}10^5$ s hold period with no additional shearing. The surfaces have abrasive wear features such as slicken lines and gouge (Figure 5a). Evidence of dissolution is present in the form of curved grain boundaries and wide cracks on many plagioclase grains (Figure 5b) as well as possible etching and pitting of grains (Figure 5c). The presence of fibrous minerals with elevated aluminum concentration (based on energy dispersive spectroscopy) on some grains shows that precipitation of secondary minerals is also occurring (Figure 5d), mostly near the outlet borehole.

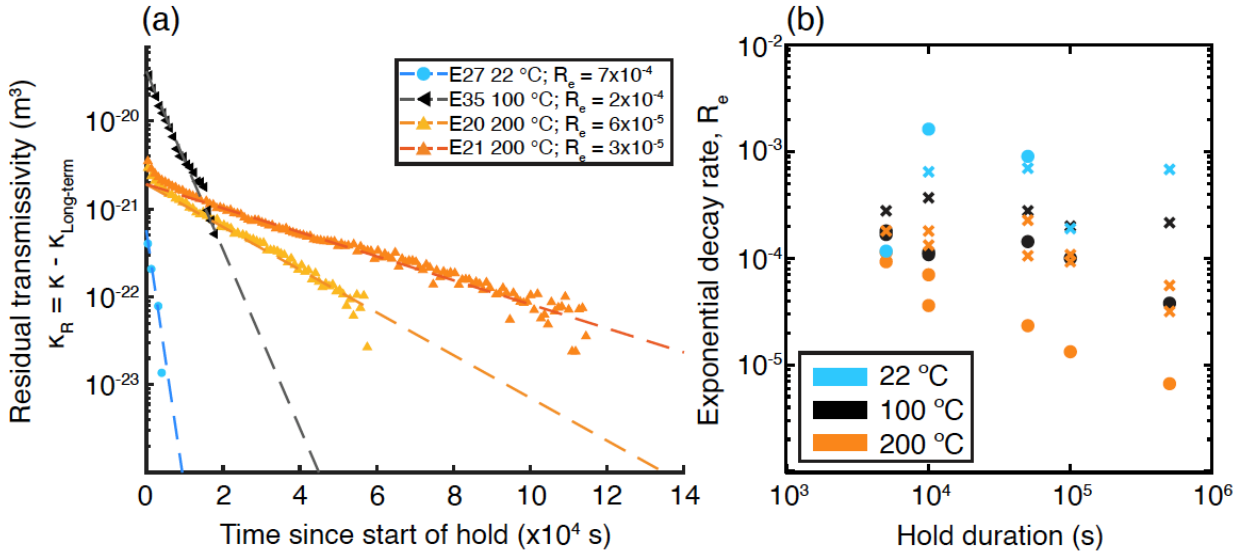

Figure 3. (a) Residual transmissivity after removal of the long-term decay trend at the beginning of the $5x10^5$ s hold indicated by the red box on Figure 2 at 22 ˚C (blue), 100 ˚C (black), and 200 ˚C (orange). The short-term decay in transmissivity at the beginning of each hold follows an exponential decay curve (Eqn. 4, dashed lines). The exponential decay rate (b) exhibits a negative correlation with temperature. The first sequence of holds, conducted at experiment times less than $6.8x10^5$ s, are indicated by x's while later holds are indicated by circles. As the first sequence of holds was conducted during the initial rapid decrease in transmissivity, which may influence the documented decay rate, the decay rates associated with the later holds are likely more representative.

4. DISCUSSION

At all temperatures examined in this study we consistently observe an overall decrease in hydraulic transmissivity with time during slide-hold tests (Figure 2), and the highest reduction rates occur during the initial 3 to 15 hours (10,800 to 54,000 s) of an experiment (Figure 2). The initial rapid loss of transmissivity is consistent with previous room temperature laboratory sliding experiments on Coulomb materials (Crawford et al., 2008; Faulkner et al., 2018; Im et al., 2018, 2019) and reflects the effects of mechanical processes such as shearing of surface asperities and development and comminution of wear products. The transition to a slower loss rate at long time scales is consistent with observations that the rate of porosity and permeability reduction in gouges slows with increasing shear strain (Crawford et al., 2008). The timing of the transition may reflect the time required for the generated wear products to achieve the "ideal" gouge fractal distribution (Biegel et al., 1989) and/or shear localization (Marone and Kilgore, 1993; Zhang and Tullis, 1998; Scuderi et al., 2017). Further slip then results in relatively little additional comminution (Mair and Abe, 2008, 2011) and any further reductions in transmissivity must occur through other means. The positive correlation between the long-term loss rate and temperature in our experiments (Figure 2b) is consistent with thermally activated hydrothermal processes such as pressure solution at grain-to-grain contacts (de Boer, 1977; Tada and Siever, 1989), stress corrosion cracking (Meredith and Atkinson, 1985; Schutjens, 1991; Heap et al., 2009), and mineral precipitation (Moore et al., 1994). At room temperature, the dissolution rate of quartz in deionized water is very slow (van Lier et al., 1960), making it unlikely that pressure solution and mineral precipitation are causing the long-term reduction observed in our experiments at 22 ˚C, so this reduction may be due to compaction driven by stress corrosion cracking at grain-to-grain contacts. Work by Yasuhara and Elsworth (2008) indicates that compaction via stress corrosion will occur at significantly faster rates than compaction due to pressure solution for temperatures up to at least 150 ˚C. It is therefore possible that the decay at 100 ˚C is also due to stress corrosion. In room-temperature experiments on Green River shale similar to those we present here, Im et al. (2019) reported a similar power law decay in permeability with power exponents of ~0.2 to 0.4, comparable to the range of power exponents we find at 22 and 100 ˚C. Im et al. (2019) also concluded that the reduction in permeability was due to stress corrosion. The increased rate of decay at 200 ˚C in our experiments may also reflect the effects of stress corrosion, as the yield strength of granular quartz powders under comparable hydrothermal conditions decreases with increasing temperature (Karner et al., 2008). However, the SEM images (Figure 5) show that dissolution and mineral precipitation are also occurring in our experiments. The greater reduction in hydraulic transmissivity at 200 ˚C may thus be the result of compaction, due to stress corrosion cracking aided by intergranular pressure solution (*e.g.,* Yasuhara and Elsworth, 2004; 2008), as well as precipitation sealing (*e.g.,* Olsen et al., 1998). The high aluminum concentration in the secondary mineral precipitates observed after a slide-hold experiment at 200 ˚C (Figure 5d) may indicate the development of kaolinite, which could further enhance the rate of transmissivity reduction by partially obstructing fluid-flow pathways.

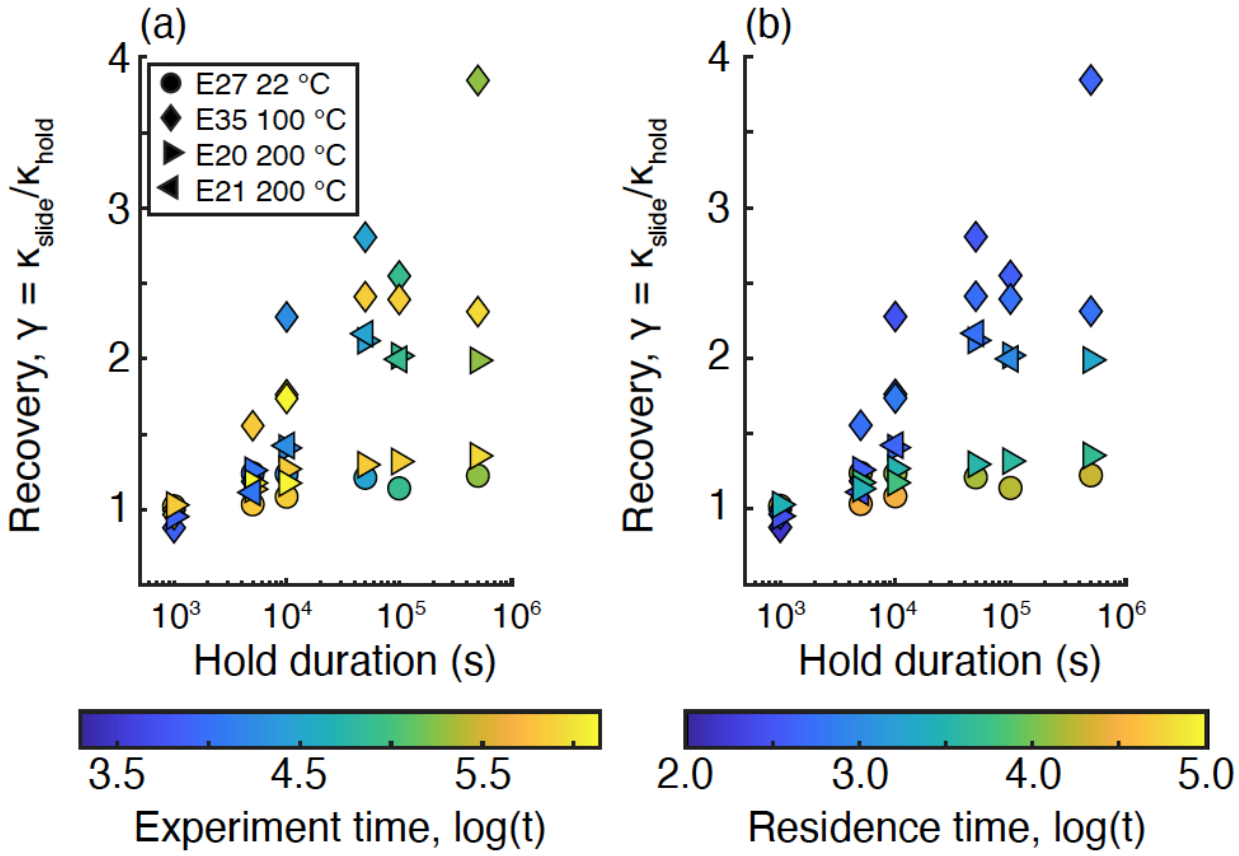

Figure 4. Recovery of hydraulic transmissivity versus hold duration. Colors indicate (a) experiment time and (b) residence time (amount of time the pore fluid is in contact with the rock). Recovery is similar at all temperature for hold durations less than 1x10^4 s but diverges for longer hold periods. Recovery is lower when residence time is greater than ~30 minutes (log(t) = 3.3).

The inverse relationship between the transient transmissivity decay rate and temperature immediately following sliding (Figure 3) is surprising. The increase in hydraulic transmissivity that occurs during the sliding is due to shear dilation (Ryan et al., 2018; Im et al., 2019), but when shear halts, it was expected that the thin gouge layer would compact via the processes discussed in the previous paragraph, and the rate would exhibit a positive correlation with temperature. That the opposite relation occurs suggests that a different process may be affecting the transient decay of hydraulic transmissivity. This inverse relationship between decay rate and temperature is also suggested by the timing of the transition from initial rapid decay to the slower long-term decay observed in Figure 2, which occurs after 3 hours at 22 ˚C and after 15 hours at 200 ˚C. A possible explanation is that the short time scale transient decays early in each experiment are due to dominantly mechanical processes (i.e., comminution, compaction), with a transition to chemo-mechanical processes at longer total elapsed times. Alternatively, as porosity is higher immediately following the end of sliding than it is later in the hold period, the difference in the decay behavior may indicate that mechanisms controlling the long-term behavior depend on the porosity, or mechanical equilibrium, of the gouge layer.

The recovery of hydraulic transmissivity that occurs with the onset of shearing is expected based on previous experiments at room temperature (Im et al., 2018, 2019). In those studies, the magnitude of recovery also increased with duration of the preceding hold period (Im et al., 2019). Olsen et al. (1998) did measure increases in permeability during sliding at hydrothermal conditions, but the magnitude of increase was not correlated with hold duration. The experiments in the current study and those of Im et al. (2019) were conducted on initially bare surface fractures, which develop a thin layer of very fine gouge, while Olsen et al.'s (1998) experiments were conducted on thick (3.5 mm) layers composed of coarse-grained (210-500 μm particle diameter) gouge. This coarser and thicker gouge may not have achieved mechanical equilibrium (Biegel et al., 1989; Zhang and Tullis, 1998) or chemical equilibrium with the pore fluid (Porter and James, 1986), which may explain why Olsen et al. (1998) did not find a correlation between permeability recovery and hold duration.

Assuming the higher rates of long-term hydraulic transmissivity reduction at elevated temperatures indicates greater fluid-assisted compaction and precipitation sealing during the hold periods, then the lower magnitude of recovery at 22 ˚C than at 100 ˚C would be expected if recovery is also controlled by pre-slip compaction and sealing (Im et al., 2018, 2019). However, the two different trends in recovery at 200 ˚C are not fully consistent with this hypothesis because the greatest reduction in transmissivity, and by inference sealing, is observed at 200 ˚C but not the greatest magnitude of recovery. Recovery at 200 ˚C is correlated with both hold duration and the amount of time the experiment has been running. As the flow rate is also decreasing the longer the experiment is running, recovery is correspondingly correlated with the amount of time the pore fluid has been in contact with the rock (*i.e.* residence time) (Figure 4b).

Greater magnitudes of hydraulic transmissivity recovery are observed at 200 ˚C when the residence time is less than 2,000 s (log(residence time) = 3.3 or ~ 30 minutes). The correlation with residence time suggests that the difference in recovery may be tied to the degree of disequilibrium between the pore fluid and rock. The time required to approach chemical equilibrium at a given temperature depends on the grain size (*ie*, surface area) and thickness of the gouge (Porter and James, 1986). For a pure quartz system composed of a 10 μm thick layer of 1 μm diameter gouge particles covering the fracture surface the pore fluid and rock should approach chemical equilibrium after about 30 minutes at 200 ˚C (Rimstidt and Barnes, 1980). The higher recovery of transmissivity associated with lower fluid residence times (< 30 minutes) at 200 ˚C (Figure 4b, experiment E20) may thus result from increased dissolution during the hold period. As the system approaches chemical equilibrium, the rate of dissolution and magnitude of recovery would decrease. It would take about 1 hour to approach chemical equilibrium at 100 ˚C, and since the residence times during experiment E35 are always less than 1 hour the recovery rate for that experiment should be particularly rapid, as observed (Figure 4b). At 22 ˚C it would take much longer to reach chemical equilibrium (> 80 hrs), but dissolution would likely be so slow at 22 ˚C that it might not have a significant impact at the time scales of the experiment, leading to low recovery regardless of chemical equilibration times.

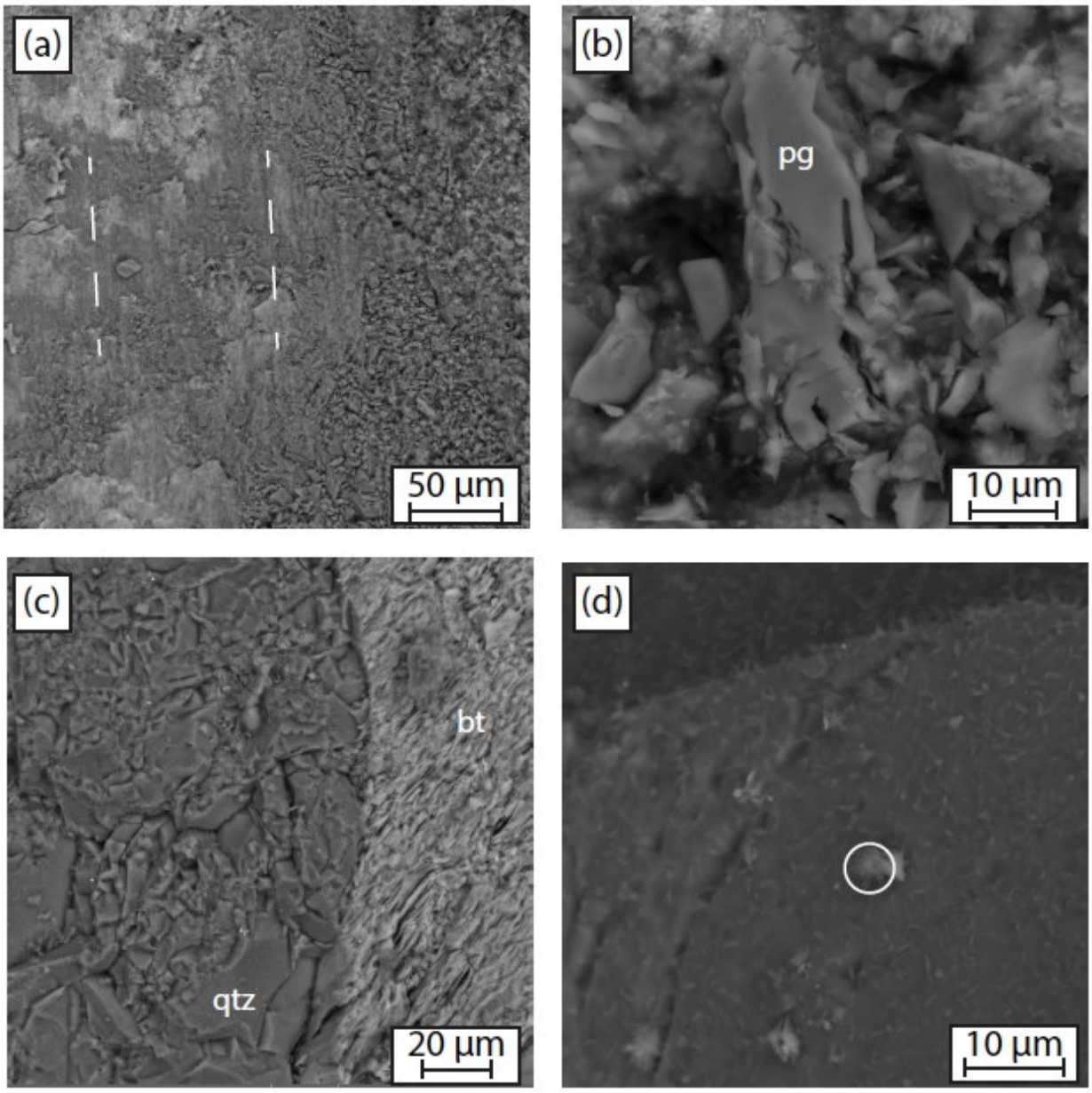

Figure 5. Scanning electron microscope (SEM) photomicrographs showing sawcut surface after 0.97 mm of slip and a 1.43x10^5 s hold at 200 ˚C. (a) The surface shows abrasive wear features such as slicken lines (white dashed lines) and ultrafine-grained gouge. White dashed lines indicate orientation of slicken lines. Evidence of dissolution is present in the form of (b) rounded grain surfaces and widened cracks on many plagioclase grains, as well as possible (c) etching and pitting of grains. (d) Secondary fibrous mineral precipitation on a quartz grain. The largest example of this mineral is circled but smaller growths cover most of the grain surface. Plagioclase = pg, Quartz = qtz, biotite = bt.

5. CONCLUSIONS

We have presented the results of experiments showing how hydraulic transmissivity evolves over a series of slide and hold periods at temperatures ranging from 22 to 200 °C. During the hold periods, transmissivity decreases leading to an overall reduction in transmissivity over the course of the experiments. The long-term reduction follows a power law decay with an exponent that increases in magnitude with increasing temperature. Superimposed on the long-term decay curve are transient increases in hydraulic transmissivity. These increases occur due to shear dilation during the sliding periods and the magnitude of transmissivity recovery appears to be related to both hold duration and the degree of chemical disequilibrium between the pore fluid and the rock. When sliding is halted, these increases in hydraulic transmissivity decay rapidly during the subsequent hold period, following an exponential decay, but the rate of decay is negatively correlated with temperature. These preliminary results suggest that when the gouge along shear fractures in geothermal systems is far from mechanical and chemical equilibrium (*e.g.,* due to continuing grain size reduction and shear dilatation), initial reductions in fracture hydraulic transmissivity may be dominated by a different mechanism from the long-term compaction mechanism.

ACKNOWLEDGMENTS AND DISCLAIMERS

This material is based upon work supported by the Department of Energy, Office of Energy Efficiency and Renewable Energy (EERE), under Award Number DE-EE0007080. This report was prepared as an account of work sponsored by an agency of the United States Government. Neither the United States Government nor any agency thereof, nor any of their employees, makes any warranty, express or implied, or assumes any legal liability or responsibility for the accuracy, completeness, or usefulness of any information, apparatus, product, or process disclosed, or represents that its use would not infringe privately owned rights. Any use of trade, firm, or product names is for descriptive purposes only and does not imply endorsement by the U.S. Government. The data presented in this paper can be found in Jeppson et al. (2023) https://doi.org/10.5066/P9NZZVD8.

REFERENCES

Acosta, M., Maye, R., and Violay, M.: Hydraulic Transport Properties of Calcite Bearing Faults with Customized Roughness: Revisiting Hydro-Shear Stimulation Techniques, Proceedings, 47th Workshop on Geothermal Reservoir Engineering, Stanford University, Stanford, CA (2022).

Biegel, R.L., and Sammis, C.G.: The Frictional Properties of a Simulated Gouge Having a Fractal Particle Distribution, Journal of Structural Geology, 11, (1989), 827-846.

Chabora, E., Zemah, E., Spielman, P., Drakos, P., Hickman, S., Lutz, S., Boyle, K., Falconer, A., Robertson-Tait, A., Davatzes, N.C., Rose, P., Majer, E., and Jarpe, S.: Hydraulic Stimulation of the Well 27-15, Desert Peak Geothermal Field, Nevada, USA, Proceedings, 37th Workshop on Geothermal Reservoir Engineering, Stanford University, Stanford, CA (2012).

Crawford, B.R., Faulkner, D.R., and Rutter, E.H.: Strength, Porosity, and Permeability Development During Hydrostatic and Shear Loading of Synthetic Quartz-Clay Fault Gouge, Journal of Geophysical Research, 113, (2008).

de Boer, R.B.: Pressure Solution: Theory and Experiments, Tectonophysics, 39, (1977), 287-301.

Fang, Y., Elsworth, D., Wang, C., Ishibashi, T., and Fitts, J.: Frictional Stability-Permeability relationships for Fractures in Shales, Journal of Geophysical Research: Solid Earth, 122, (2017), 1760-1776.

Farough, A., Moore, D.E., Lockner, D.A., and Lowell, R.P.: Evolution of Fracture Permeability of Ultramafic Rocks Undergoing Serpentinization at Hydrothermal Conditions: An Experimental Study, Geochemistry, Geophysics, Geosystems,17, (2016), 44-55.

Faulkner, D.R., Sanchez-Roa, C., Boulton, C., and den Hartog, S.A.M.: Pore Fluid Pressure Development in Compacting Fault Gouge in Theory, Experiments, and Nature, Journal of Geophysical Research: Solid Earth, 123, (2018), 226-241.

Hantush, M.S.: Hydraulics of Wells, in Advances in Hydroscience, vol. 1, ed. V.T. Chow, (1964), 282-433.

Heap, M.J., Baud, P., and Meredith, P.G.: Influence of Temperature on Brittle Creep in Sandstones, Geophysical Research Letters, 36, (2009).

Hickman, S., Zoback, M.D., and Benoit, R.: Tectonic Controls on Fault-Zone Permeability in a Geothermal Reservoir at Dixie Valley, Nevada, in Rock Mechanics in Petroleum Engineering, vol. 1, R. M. Holt (ed.), Society of Petroleum Engineers, SPE-47213-MS (1998).

Im, K., Elsworth, D., and Fang, Y.: The Influence of Preslip Sealing on the Permeability Evolution of Fractures and Faults, 45, (2018), 166-175.

Im, K., Elsworth, D., and Wang, C.: Cyclic Permeability Evolution During Repose Then Reactivation of Fractures and Faults, Journal of Geophysical Research: Solid Earth, 124, (2019). 4492-4506.

Jeppson, T., Lockner, D., Taron, J., Moore, D., Kilgore, B., Beeler, N., and Hickman, S. (2023) Data release for "Effect of thermal and mechanical processes on hydraulic transmissivity evolution", U.S. Geological Survey data release, https://doi.org/10.5066/P9NZZVD8.

Karner, S.L., Kronenberg, A.K., Chester, F.M., Chester, J.S., and Hajash, A.: Hydrothermal Deformation of Granular Quartz Sand, Journal of Geophysical Research, 113, (2008).

Kitagawa, Y., Fujimori, K., and Koizumi, N.: Temporal Change in Permeability of the Nojima Fault Zone by Repeated Water Injection Experiments, Tectonophysics, 443, (2002), 183-192.

Lockner, D.A., Kilgore, B.D., Beeler, N.M., and Moore, D.E.: The Transition from Friction Sliding to Shear Melting in Laboratory Stick-Slip Experiments, Fault Zone Dynamic Processes: Evolution of Faut Properties During Seismic Rupture, (2017), 105-131.

Mair, K., and Abe, S.: 3D Numerical Simulations of Fault Gouge Evolution During Shear: Grain Size Reduction and Strain Localization, Earth and Planetary Science Letters, 274, (2008), 72-81.

Mair, K., and Abe, S.: Breaking Up: Comminution Mechanisms in Sheared Simulated Fault Gouge, Pure and Applied Geophysics, 168, (2011), 2277-2288.

Manga, M., Beresnev, I., Brodsky, E.E., Elkhoury, J.E., Elsworth, D., Ingebritsen, S.E., Mays, D.C. and Wang, C.Y.: Changes in Permeability Caused by Transient Stresses: Field Observations, Experiments, and Mechanisms, Reviews of Geophysics, 50. (2012).

Marone, C., and Kilgore, B.: Scaling of the Critical Slip Distance for Seismic Faulting with Shear Strain in Fault Zones, Nature, 362, (1993), 618-621.

Meredith, P.G., and Atkinson, B.K.: Fracture Toughness and Subcritical Crack Growth During High-Temperature Tensile Deformation of Westerly Granite and Black Gabbro, Physics of the Earth and Planetary Interiors, 39, (1985), 33-51.

Moore, D.E., Lockner, D.A., and Byerlee, J.D.: Reduction of Permeability in Granite at Elevated Temperatures, Science, 265, (1994), 1558-1561.

Morrow, C.A., Moore, D.E., and Lockner, D.A.: Permeability Reduction in Granite Under Hydrothermal Conditions, Journal of Geophysical Research, 106, (2001), 30551-30560.

Olsen, M.P., and Scholz, C.H.: Healing and Sealing of a Simulated Fault Gouge Under Hydrothermal conditions: Implications for Fault Healing, Journal of Geophysical Research, 103, (1998), 7421-7430.

Plummer, M., Bradford, J., Moore, J., and Podgorney, R.: Reservoir Response to Thermal and High-Pressure Well Stimulation Efforts at Raft River, Idaho, No. INL/CON-16-39543. Idaho National Lab, Idaho Falls, ID (2016).

Polak, A., Elsworth, D. Yasuhara, H., Grader, A.S., and Halleck, P.M.: Permeability Reduction of a Natural Fracture Under Net Dissolution by Hydrothermal Fluids, 20, (2003).

Porter, E.W., and James, W.C.: Influence of Pressure, Salinity, Temperature, and Grain Size on Silica Diagenesis in Quartzose Sandstones, Chemical Geology, 57, (1986), 359-369.

Rimstidt, J. D., and Barnes, H. L.: The Kinetics of Silica-Water Reactions, Geochimica et Cosmochimica Acta, 44, (1980), 1683-1699.

Ryan, K.L., Rivière, J., and Marone, C.: The Role of Shear Stress in Fault Healing and Frictional Aging, Journal of Geophysical Research: Solid Earth, 123, (2018), 10479-10495.

Schutjens, P.M.T.M.: Experimental Compaction of Quartz Sand at Low Effective Stress and Temperature Conditions, Journal of the Geological Society, London, 148, (1991), 527-539.

Scuderi, M.M., Collettini, C., Viti, C., Tinti, E., and Marone, C.: Evolution of Shear Fabric in Granular Fault Gouge from Stable Sliding to Stick Slip and Implications for Fault Slip Mode, Geology, 45, (2017), 731-734.

Tada, R., and Siever, R.: Pressure Solution During Diagenesis, Annual Review of Earth and Planetary Sciences, 17, (1989), 89-118.

Tenthorey, E., Cox, S.F., and Todd, H.F.: Evolution of Strength Recovery and Permeability During Fluid-Rock Reaction in Experimental Fault Zones, Earth and Planetary Science Letters, 206, (2003), 161-172.

van Lier, J.A, de Bruyn, P.L., and Overbeek, J.T.G.: The Solubility of Quartz, The Journal of Physical Chemistry, 64, (1960), 1675-1682.

Xue, L., Li, H.-B., Brodsky, E.E., Xu, Z.-Q., Kano, Y., Wang, H., Mori, J.J., Si, J.-L., Pei, J.-L., Zhang, W., Yang, G., Sun, Z.-M., and Huang, Y.: Continuous Permeability Measurements Record Healing Inside the Wenchuan Earthquake Fault Zone, Science, 340, (2013), 1555-1560.

Yasuhara, H., and Elsworth, D.: Evolution of Permeability in a natural Fracture: Significant Role of Pressure Solution, Journal of Geophysical Research, 109, (2004).

Yasuhara, H., and Elsworth, D.: Compaction of a Rock Fracture Moderated by Competing Roles of Stress Corrosion and Pressure Solution, Pure and Applied Geophysics, 165, (2008) 1289-1306.

Zhang, S., and Tullis, T.E.: The Effect of Fault Slip on Permeability and Permeability Anisotropy in Quartz Gouge, Tectonophysics, 295, (1998), 41-52.

Zhang, S., Tullis, T.E., and Scruggs, V.J.: Permeability Anisotropy and Pressure Dependency of Permeability in Experimentally Sheared Gouge Materials, Journal of Structural Geology, 21, (1999), 795-806.

Zimmerman, R.W., and Bodvarsson, G.S.: Hydraulic Conductivity of Rock Fractures, Transport in Porous Media, 23, (1996), 1-30.